ISSN 1330-3651 (Print), ISSN 1848-6339 (Online)
https://doi.org/10.17559/TV-20240712001841
Original scientific paper

Design and Performance Analysis of Dual Straight Beam MEMS Micro Mirrors for Enhanced Scanning Capabilities

Lin ZHANG, Qian WANG, Yuanlin XIA*, YanTing XIA, Lei ZHONG

Abstract: Micro-Opto-Electro-Mechanical Systems (MOEMS) technology is rapidly developing, with micro scanning devices centered around MEMS micro-mirrors increasingly becoming a research focus. Addressing the shortcomings of single-cantilever MEMS micro-mirrors, which suffer from high beam stress, small scanning angles, and inadequate frequency response, the study proposes a novel dual axis micro mirror with a dual straight beam structure to address limitations in current MEMS micro mirror designs. Using COMSOL finite element software, we optimized the structural dimensions and conducted performance simulations. The proposed design achieves a fast axis resonant frequency of 4397 Hz with a maximum scanning angle of 31°, and a slow axis resonant frequency of 422.3 Hz with a maximum scanning angle of 50.2°. Compared to single beam structures, our design demonstrates 17.2% and 18.7% stress reduction for fast and slow axis scanning respectively, under equivalent deflection. This dual straight beam MEMS micro mirror offers improved mechanical deflection performance, reduced crosstalk, and enhanced scanning capabilities, contributing to advancements in optical systems and scientific exploration.

Keywords: dual straight beam; electromagnetic Drive; MEMS Micro Mirrors Stress

1 INTRODUCTION

The MEMS Micro Scanning Mirror (commonly known as MEMS micro-mirrors) is a quintessential example of a micro-opto-electromechanical system. Through precise control of their translational or rotational movements, these micro-mirrors can perform a variety of functions such as focusing, defocusing, reflecting, and modulating the frequency and amplitude of incident light, thereby facilitating the scanning process [1-3]. MEMS mirrors play a crucial role in advancing the development and innovation of optical technology due to their key characteristics. These include providing precise beam control in optical systems, rapid response, miniaturized integration, cost-effectiveness, programmability, environmental stability, and the capability for multi-wavelength operation. MEMS micro mirrors are divided into one-dimensional and two-dimensional types based on scanning dimensions and into four categories: electrostatic, electrothermal, piezoelectric, and electromagnetic, by driving method [4, 5]. Electrostatic models, though mature, have high driving voltages and nonlinear responses. Electrothermal models respond slowly and are sensitive to external factors. Piezoelectric models, due to their driving principle, have limited displacement and are not suitable for wide-range scanning. Electromagnetic models, however, operate at low voltages, provide strong driving forces, enable significant displacements, and allow for large scanning angles [6, 7].

Owing to the structural complexity of the micro-mirrors and the properties of the materials used, it typically exhibits a highly underdamped system, resulting in a deficient dynamic response and limited positioning accuracy [8]. The reflective surface typically measures 3 to 5 millimeters in diameter, with a common single beam torsion structure having a thickness and width of 200 to 500 micrometers [9-11]. This micro-design challenges the material's stress endurance. Stress constraints limit the torsion angle; excessive angles risk beam damage or fracture, thus restricting the scanning angle range [12, 13]. In 2014, M. Pallapa and colleagues developed a low-cost, low-voltage, and large scanning angle electromagnetic MEMS micro-mirrors using magnetic film, mirror, torsion beam, frame, and planar drive coil, achieving a compact size [14]. In 2016, Zhou Ying and others utilized micro-nano processing techniques to create an electromagnetic scanning grating micro-mirror chip, enabling the substitution of a single-tube detector for an array [15]. In 2023, Wu Jiaqi and colleagues designed an electrostatic-driven parallel plate micro-mirror that, with the same driving force, achieves greater vertical displacement through structural enhancements [16]. Overall, micro-nano processing technology has made MEMS micro-mirrors even smaller, but it also poses challenges in terms of the beam structure's stress endurance. Excessive torsion angles may cause damage to the beams, limiting the performance of the micro-mirrors. The design of the dual straight beam torsion structure, by distributing the load, reduces the stress on individual beams and prevents damage, thereby increasing the torsion and scanning angles. This compensates for the stress deficiency brought about by miniaturization.

Regarding the above issues, the paper presents an electromagnetic-driven MEMS dual straight beam scanning micro-mirror that utilizes the interaction force between a current carrying coil and a permanent magnet to achieve scanning. The paper first conducts an in-depth analysis of the driving mechanism and torsional dynamics of the MEMS micro-mirrors. Subsequently, the structural dimensions of the micro-mirror are designed and optimized using COMSOL finite element software. Through modal simulation analysis, harmonic response simulation analysis, and ultimate simulation stress, a comparative performance analysis is conducted between the dual straight beam structure and the single straight beam structure micro-mirrors. Through this research, we aim to provide new insights and solutions for the design and application of MEMS micro-mirrors.

2 METHODS AND EXPERIMENTS

2.1 Actuation Method

The electromagnetic actuation of the MEMS biaxial scanning micro-mirror primarily relies on the interaction between the electrified coil and the permanent magnet's electric field for scanning. When a current of a specific frequency is applied to the *X* and *Y* axis drive coils within a constant magnetic field, the drive coils experience Lorentz forces, which act as the driving force to rotate the reflector. This rotation deflects the laser beam, enabling it to traverse a predetermined scanning range, thus completing the image scan [17, 18]. The electromagnetic MEMS micro-mirror device designed in this paper consists of six parts: a rectangular cross-section torsion beam, a mirror, an inner frame, a coil embedded in the inner frame, an outer frame, and a permanent magnet. The mirror is connected to the inner frame via the torsion beam (fast axis), while the inner frame is secured to the outer frame with the torsion beam (slow axis). This paper introduces a novel actuation method using a dual straight beam supporting structure and a 45° inclined magnetic field, enabling biaxial deflection with a single drive coil, as illustrated in Fig. 1.

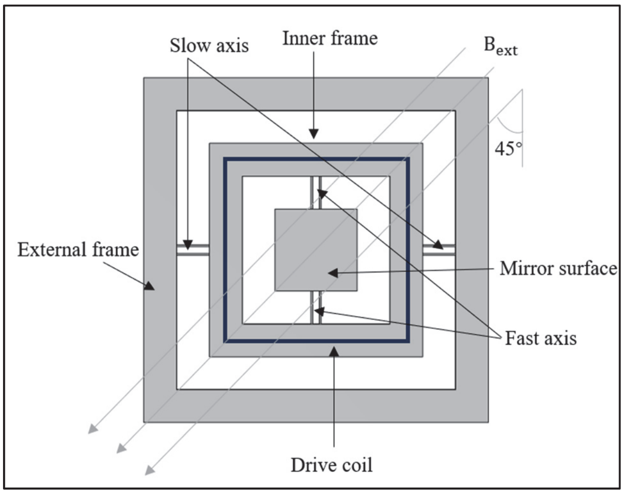

Figure 1 Dual Axis Scanning Micro-Mirror with Two Straight Beam Support

This design differs from other configurations where the magnet is positioned directly beneath the micro mirror. The micro mirror's magnet is situated around its perimeter, level with the mirror, and employs a "7" shaped magnet to maintain a 45° angle with the central axis. To ensure an adequate driving force, the inner frame integrates numerous rectangular driving coils. In the dual axis scanning micro-mirror structure supported by two straight beams, a current excitation signal at a specific frequency is applied to the driving coil. This energized coil experiences Lorentz force within a constant magnetic field [19-21]. Owing to the coil's embedding in the inner frame, the resultant torque influences the inner frame, inducing rotation of the outer torsion beam (slow axis). Resonance is achieved by exciting the natural frequency, thereby enhancing the amplitude of oscillation and facilitating the rotation of the inner torsion beam (fast axis). A single coil and a 45° oblique magnetic field facilitate rapid scanning around the fast axis and slower scanning around the slow axis of the micro mirror, as illustrated in Fig. 2.

The laser beam is directed at the MEMS micro mirror's surface, which rotates along both axes. This rotation results in a defined rectangular scanning field angle, enabling both horizontal and vertical scanning. The force on a single-turn rectangular coil is analyzed, and the magnitude of the Lorentz force on a biaxial scanning micro-mirror supported by two straight beams is calculated. The force dynamics in a constant magnetic field are illustrated in Fig. 3.

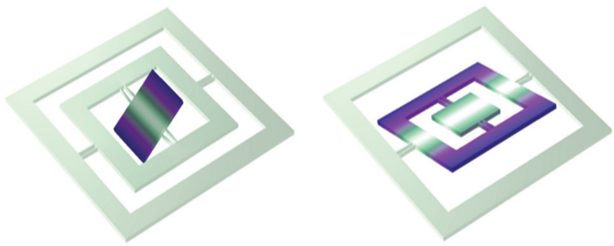
Figure 2 The excitation signal drives the mirror to rotate along two axes

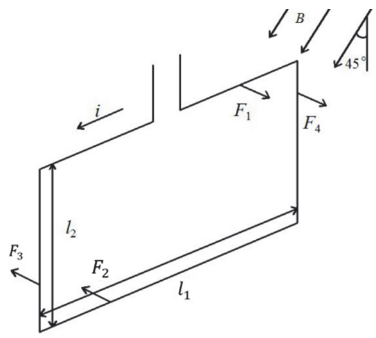

Figure 3 The excitation signal drives the mirror to rotate along two axes

Consider the coil as a rectangular one, with the lengths of its upper and lower sides being l_1, and those of its left and right sides also being l_2. The magnetic induction intensity is denoted as *B*, with a direction at a 45° angle to the vertical. The magnetic induction lines are resolved along the upper and right edges of the rectangular coil. The forces exerted on each of the coil's upper, lower, left, and right sides are as follows:

$$F_1 = iBl_1 \sin 45° \tag{1}$$

$$F_2 = iBl_1 \sin 45° \tag{2}$$

$$F_3 = iBl_2 \sin 45° \tag{3}$$

$$F_4 = iBl_2 \sin 45° \tag{4}$$

Eq. (1) to Eq. (4) indicate that the forces on the upper and lower sides of the rectangular coil are equal and opposite, and those on the left and right sides are as well. Consequently, F_1 and F_2 on the upper and lower sides will generate a torque T_1, while F_3 and F_4 on the left and right sides will produce another torque T_2. The magnitudes of T_1 and T_2 can be determined as follows:

$$T_1 = \frac{F_1 l_2}{2} + \frac{F_2 l_2}{2} = iBS \sin 45° \tag{5}$$

$$T_2 = \frac{F_3 l_1}{2} + \frac{F_4 l_1}{2} = iBS \sin 45° \tag{6}$$

where *S* represents the coil area. Eq. (5) and Eq. (6) reveal that T_1 is directed outward and T_2 inward. Energizing the coil results in identical torques on both the upper and lower, and the left and right sides of the inner frame. Electromagnetically actuated MEMS mirrors in practical applications integrate multi-turn coils to generate substantial driving forces. Assuming the aforementioned coil is the innermost one, with uniform coil spacing of δ, and a total of N turns, the side lengths of the innermost coil are l_1 and l_2 respectively. The total driving torque can be calculated using Eq. (5) and Eq. (6):

$$T_{1\text{total}} = T_{2\text{total}} = iB\sin 45° \sum_{m=0}^{N-1} \left(l_1 + 2N\delta\right)\left(l_2 + 2N\delta\right) \tag{7}$$

Eq. (7) shows that the torque is influenced by factors such as coil current intensity, magnetic induction intensity of the constant magnetic field, number of coil turns, and coil area. The coil integrated within the inner frame experiences a resultant torque with a known magnitude and direction. Given the coil's fixed connection to the inner frame, it effectively subjects the inner frame to a closing torque.

2.2 Dynamic Model

The drive coil experiences a torque due to the periodic variation of the constant magnetic field, which acts on the inner frame and causes the torsion beam connected to it to twist, thereby driving the reflector and the outer frame to twist.

The torsional dynamic model is a standard mass-spring-damping second-order vibration system [22, 23], described by the differential equation of motion:

$$J\ddot{\theta} + C\dot{\theta} + K\theta = T \tag{8}$$

where J represents the rotational inertia of the micro-mirror, K denotes the torsional stiffness of the torsion beam, C is the system damping coefficient, T is the electromagnetic driving torque, and θ is the rotation angle of the micro-mirror. The structure of the torsion beam dictates the torsional stiffness K of the torsion beam, where T is related to the number of turns of the driving coil, the driving current, and the intensity of the external magnetic field, among other factors. Three points are selected on the micro-mirror to represent three types of motion, as illustrated in Fig. 4.

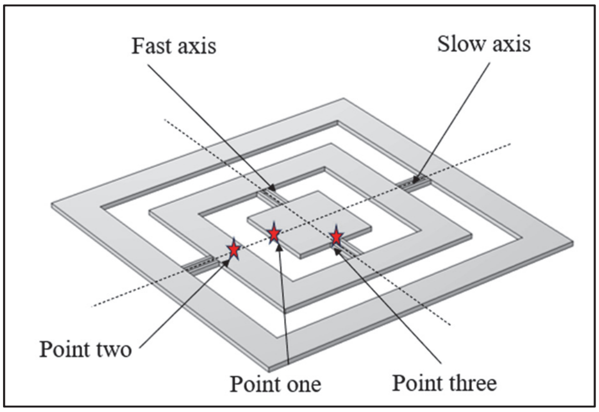

Figure 4 Location of motion analysis points

Let point 1 swing angle around the fast axis be θ, point 2 be θ_1, and point 3 be θ_2 around the slow axis. Point 1 represents the mirror surface, while points 2 and 3 represent the inner frame. The inner frame is subjected to a torque, causing the micro-mirror to rotate along the slow axis. Since the inner mirror surface is not subjected to force, it rotates along the fast axis. The motion equations for points 1, 2, and 3 are as follows:

$$J\ddot{\theta} + C\dot{\theta} + K\left(\theta - \theta_1\right) = 0 \tag{9}$$

$$J_1\ddot{\theta}_1 + C_1\dot{\theta}_1 + \left(K_1 + K\right)\theta_1 = T + K\theta \tag{10}$$

$$J_2\ddot{\theta}_2 + C_2\dot{\theta}_2 + K_2\theta_2 = T \tag{11}$$

where C_i is the damping coefficient for the ith point. Assuming the angular velocity as: $\varphi_1 = \dot{\theta}$, $\varphi_2 = \dot{\theta}_1$, $\varphi_3 = \dot{\theta}_2$,the aforementioned motion equations, expressed in the frequency domain, facilitate the construction of a transfer matrix between force, torque, and angular velocity:

$$\begin{bmatrix} sJ + C + \frac{K}{s} & -\frac{K}{s} & 0 \\ -\frac{K}{s} & sJ_1 + C_1 + \frac{K_1 + K}{s} & 0 \\ 0 & 0 & sJ_2 + C_2 + \frac{K_1}{s} \end{bmatrix} \times \begin{bmatrix} \varphi_1 \\ \varphi_2 \\ \varphi_3 \end{bmatrix} = \begin{bmatrix} 0 \\ T \\ T \end{bmatrix} \tag{12}$$

The relationship between the velocities of Point 1 and Point 2 is derived from Eq.(12). The angular velocity of the endoscope surface around the fast axis differs from that of the inner frame. Due to mechanical constraints, the endoscope may lag or lead the inner frame in its motion. Although the driving coil does not directly apply force to the endoscope, the endoscope surface may exhibit a relative angular deviation from the inner frame. When the excitation signal meets certain criteria, the endoscope surface may also oscillate around the fast axis, a motion facilitated by the structure's inherent characteristics. Based on the principle of combined actuation by a 45° oblique magnetic field and a coil, when two sinusoidal signals at the resonant frequency are applied to the driving circuit interface, the superimposed driving torque is resolved into forces that cause rotations along the fast and slow axes. This is achieved through mechanical decoupling, enabling movements along both axes.

2.3 Model Establishment

The MEMS micro-mirror utilizes the torsion of a torsion beam to rotate the mirror surface. If the mirror is too thin, it may undergo deformation during torsion, compromising the optical performance of the micro-mirror. Therefore, specific requirements are imposed on the thickness of the micro-mirror. In this study, 500 μm thick anisotropic monocrystalline silicon is employed to fabricate the substrate of the MEMS micro-mirror using etching techniques. A dual straight beam supporting structure, distinct from the traditional single straight beam design, is developed. Both single straight beam and dual straight beam models are established. The torsion beams of both structures have the same cross-sectional area, as illustrated in Fig. 5.

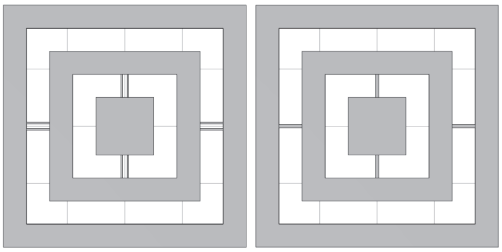

Figure 5 Dual Beam and Single Beam Support Models

The mapping method is employed to locally refine the mesh of the four torsion beams in the micro mirror, with the beam boundaries subjected to mesh division. Along the length of the torsion beams, 50 points are established, and 10 points are set in the width direction, dividing the beams into 50 × 10 small hexahedral elements, with the mesh element size set to "fine." The simulation results are depicted in Fig. 6.

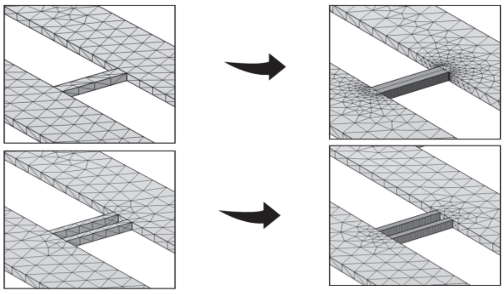

Figure 6 Grid division of dual straight beam structure

2.3.1 Structural Optimization of Beam Spacing

For the dual straight beam supporting structure, the beam spacing influences both the rotation angle and scanning frequency of the micro mirror. To identify the optimal beam spacing that ensures micro mirrors with varying spacings deflect by the same angle, a simulation analysis is conducted in COMSOL. The beam spacing for the micro mirror with a dual straight beam supporting structure is set within the range of 0.05 - 0.2 mm. The micromirror is deflected 30° along the fast axis to simulate its resonance mode, as illustrated in Fig. 7.

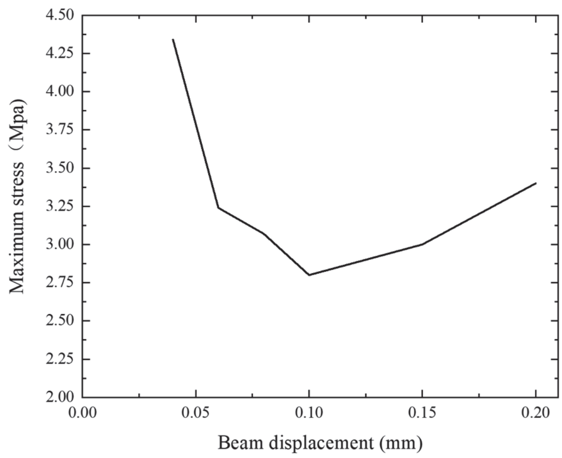

Figure 7 Relationship between beam spacing and maximum stress

Fig.7 demonstrates that the beam spacing significantly affects the torsional stress, generally decreasing initially and then increasing. The stress is minimal when the beam spacing is 0.1 mm, which is thus selected as the optimal distance between the two beams.

2.3.2 Structural Optimization of Beam Length

If the torsion beam is excessively long, it results in insufficient beam stiffness, which lowers the scanning frequency of the micro-mirror. This reduces the micro-mirror's resolution and scanning efficiency during three-dimensional scanning. Conversely, a beam that is too short leads to excessive stiffness, which in turn limits the micro-mirror's rotational angle and narrows its scanning range. The optimization method for beam length involves setting the beam width to 0.1 mm and analyzing torsion beam lengths ranging from 1 mm to 3 mm, with a 0.5 mm interval, to assess the impact of beam length on resonant frequency and scanning angle. The scanning angle θ is determined using the micro-mirror's displacement measured through simulation, according to the formula:

$$\theta = \arctan\frac{h}{l} \tag{13}$$

where h represents the vertical rotational displacement and l the horizontal rotational displacement. The simulation is illustrated in Fig. 8. As the beam length increases, the scanning frequency rises and the scanning angle narrows. For a 2 mm torsion beam length, a better resolution and wider scanning angle justify its selection.

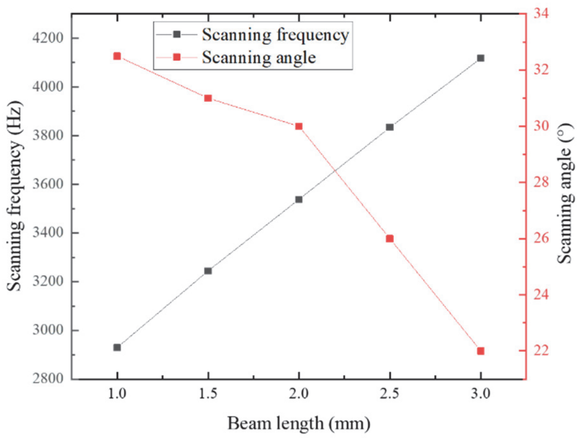

Figure 8 Relationship between beam length and scanning frequency and scanning angle

2.3.3 Structural Optimization of Beam Width

Similar to the impact of beam length on stiffness, an excessively wide torsion beam can lead to excessive stiffness, which in turn affects the rotational angle of the micro scanning mirror; an excessively narrow beam can result in insufficient stiffness, thereby reducing the scanning frequency of the micro mirror. This, in turn, diminishes the micro mirror's resolution and impairs the scanning quality during three-dimensional scanning patterns. The optimization of beam length involves setting the beam length to 2 mm and analyzing torsion beam widths within the range of 0.1 mm to 0.3 mm, with an interval of 0.05 mm. The simulation results are depicted in Fig. 9. As the beam width increases, the scanning frequency gradually rises and the scanning angle progressively decreases. At a beam width of 0.2 mm, the scanning angle is relatively large. Beyond 0.2 mm, while the scanning frequency continues to rise steadily, the scanning angle drops sharply. Consequently, the beam width is chosen to be 0.2 mm.

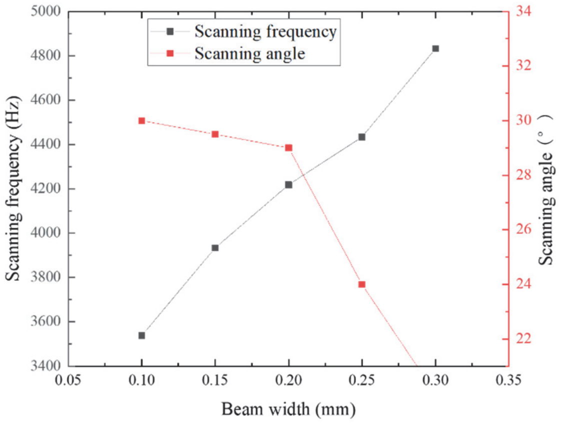

Figure 9 Relationship between beam width and scanning frequency and scanning angle

The dimensions of the micro mirror designed in this study are: a mirror size of 5 × 5 × 0.5 mm, a torsion beam length of 2 mm, a torsion beam width of 0.2 mm, and a spacing of 0.1 mm between the two torsion beams.

3 METHODS AND EXPERIMENTS

Two micro-mirrors were chosen for simulation analysis: one with a beam size of 2×0.2×0.5mm (beam spacing of 0.1mm) and another with a single beam structure and a beam size of 2×0.4×0.5mm. The performance of these micro-mirrors was compared, focusing on the advantages of the dual beam micro mirrors.

3.1 Modal Analysis

Utilize the "steady state, eigen frequency" study feature in COMSOL Multiphysics finite element simulation software to analyze the first six modes of both dual straight beam supported micro mirrors and single straight beam supported micromirrors. Refer to Fig. 10 and Fig. 11 for the corresponding results.

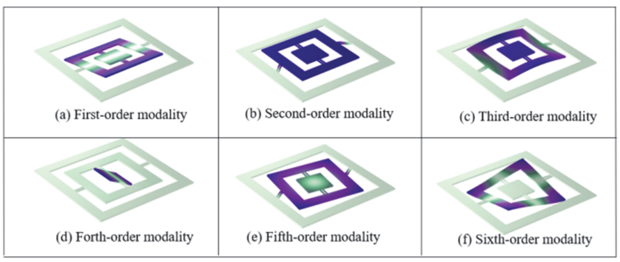

Figure 10 The first sixth-order mode of micro-mirror with dual beam structure

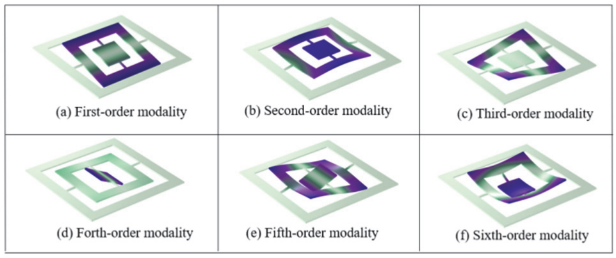

Figure 11 The first sixth-order mode of micro-mirror with single beam structure

The rotation around the slow axis is depicted in Fig. 10a as the first-order mode, while the rotation around the fast axis is illustrated in Fig.10d as the fourth-order mode. Tab. 1 presents the modal simulation data for micro-mirrors with dual and single straight beam structures, as derived from Fig. 10 and Fig. 11.

Table 1 Resonant frequency analysis data

Structure type	Scanning direction	Resonant frequency / Hz
Dual beam	fast axis	4397
	low axis	422.3
Single beam	fast axis	3371
	low axis	313.4

The resonance frequencies of the fast and slow axes for the dual straight beam supporting micro-mirrors are 4.397 kHz and 422.3 Hz, respectively. In comparison, the single straight beam supporting micro-mirror has resonance frequencies of 3.371 kHz for the fast axis and 313.4 Hz for the slow axis. The difference in resonance frequencies between the fast and slow axes is more pronounced in the dual straightbeam support configuration than in the single straightbeam support. Additionally, the crosstalk in the dual straight beam supporting micro-mirror is reduced, and its fast-axis resonance frequency is higher. Consequently, during three-dimensional scanning, this structure exhibits enhanced resolution and scanning performance.

3.2 Harmonic Response Analysis

To examine the correlation between the amplitude and frequency of a mirror rotating around an axis, a harmonic response analysis of the mirror is essential. Given the intricate interplay of the electric field, magnetic field, and solid mechanical field, the harmonic response analysis employs the torque derived from Eq. (7) to introduce a harmonic disturbance load to the internal frame of the solid mechanical field for analysis. The torque specified in Eq. (7) is influenced by factors such as the number of coil turns and spacing. Due to spatial constraints within the inner frame, integrating a multi-turn coil is challenging; hence, a torque of 2.5×10^{-2} N·m is adopted in this study. A harmonic disturbance load is imposed on the internal frame within the solid mechanics field across a frequency range from 0 to 5500 Hz. To elucidate the relationship between rotation amplitude and frequency response, two specific points, A and B, in Fig. 12 were selected for investigating the connection between their *Z*-axis displacement and frequency response.

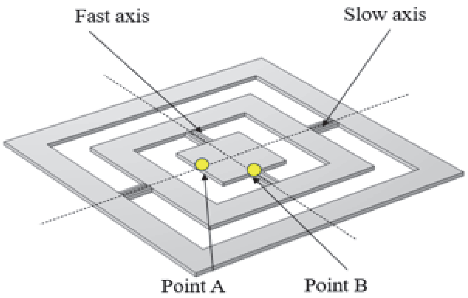

Figure 12 Positional relationship between two points A and B

The movement of point A along the Z-axis corresponds to the rotation of the micro mirror around the fast axis, while the movement of point B along the Z-axis corresponds to the rotation of the micro mirror around the slow axis. Refer to Fig. 13 for the frequency response curve.

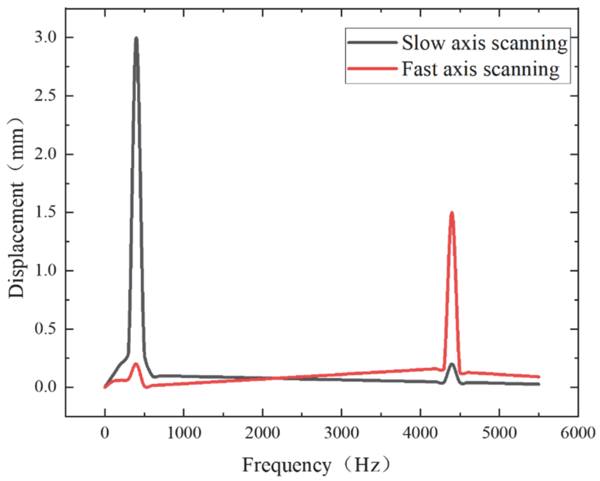

Figure 13 Harmonic response curve of dual straight beam structure

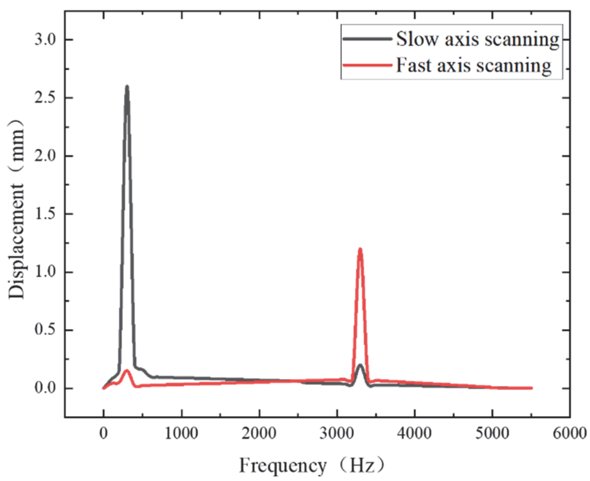

Figure 14 Harmonic response curve of single straight beam structure

The maximum angles of rotation along the fast and slow axes for the two micro-mirrors structures are determined based on the displacement data using Eq. (13). As shown in Tab. 2.

Table 2 Resonant frequency analysis data

Structure type	Scanning direction	Maximum displacement / mm	Maximum angle / °
Dual beam	fast axis	1.5	31.0
	low axis	3	50.2
Single beam	fast axis	1.2	25.6
	low axis	2.6	46.1

The data presented in Tab. 3 and Tab. 4 demonstrate that the dual straight beam supporting the micro-mirror achieves a maximum resonant displacement of 1.5 mm along the fast axis, with a corresponding maximum deflection angle of 31.0°. Along the slow axis, the maximum resonant displacement reaches 1.2 mm, with a maximum deflection angle of 25.6°. These results indicate superior harmonic response compared to the straight beam supporting structure, resulting in a broader scanning range.

3.3 Ultimate Stress

Increased rotation angle of the micro-mirror leads to higher stress on the torsional beam. To prevent torsional beam fracture resulting from stress surpassing the maximum stress of single crystal silicon, which could lead to device structure failure, stress analysis of the micro-mirror is essential. The ultimate stress of dual and single straightbeam micro-mirror structures was simulated and calculated under identical deflection angles. By applying a displacement of 0.90 mm in opposite directions to both sides of the mirror along the fast axis and to both sides of the inner frame along the slow axis, the torsion angle of the micro-mirror was simulated along both axes, as depicted in Fig.15.

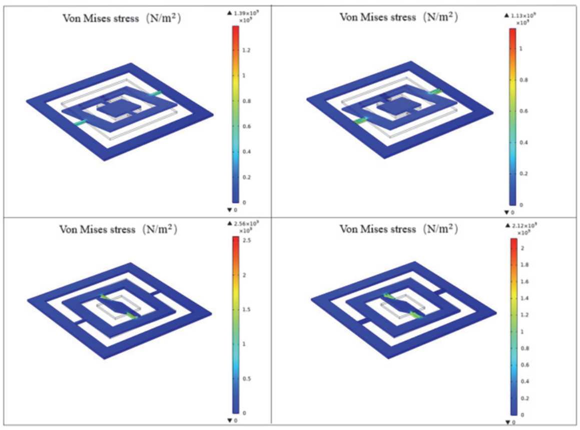

Figure 15 Stress distribution of dual and single beam structures with the same deflection angle

The stress distribution data for the micro-mirror beams in both dual and single straight beam structures can be derived from Fig. 15 and is presented in Tab. 3.

Table 3 Maximum stress on torsion beam

Structure type	Scanning direction	Maximum stress of torsion beam / GPa
Dual beam	fast axis	2.21
	low axis	1.13
Single beam	fast axis	2.56
	low axis	1.39

The stress distribution analysis of the micro-mirror supported by dual straight beams, as presented in Tab. 5 and Tab. 6, reveals that rotation around the fast axis results in stress concentration on the inner torsion beam, reaching a maximum of 2.12 GPa. Conversely, rotation around the slow axis induces stress distribution on the outer torsion beam, peaking at 1.13 GPa. In comparison to the single straight beam configuration, the maximum stresses observed are 2.56 GPa and 1.39 GPa for fast and slow axis rotations, respectively. Consequently, the stress reduction for fast axis scanning is 17.2%, and for slow axis scanning is 18.7%, relative to the single straight beam structure, under equivalent micro-mirror deflection.

4 CONCLUSION

In response to the issues of high stress, small scanning angle, and insufficient frequency response in single straight beam MEMS micro-mirrors, this study proposes a novel electromagnetic-driven dual straightbeam MEMS micro-mirror. This design achieves high-frequency resonance and large-angle scanning while meeting the size requirements of optical systems. Simulation results show that compared to the traditional single straightbeam structure, the stress on the MEMS dual straightbeam supported micro-mirrors during fast and slow-axis scanning is reduced by 17.2% and 18.7%, respectively. The scanning angle at maximum deflection displacement is increased by 21.09% and 8.89%, and the resonance frequency is increased by 30.43% and 34.74%. The research findings indicate that: (1) The dual straightbeam structure effectively reduces stress during large angle deflection, enhancing the reliability and durability of the micro-mirror. (2) The dual straight beam micro mirror exhibits superior harmonic response and a larger field-of-view scanning range on both axes. (3) Compared to the single straightbeam structure, the dual straightbeam structure has a significantly larger difference in resonance frequency between the fast and slow axes, with minimal crosstalk, and a higher fast-axis resonance frequency, which is beneficial for improving the resolution and performance of three-dimensional scanning. The proposed design's enhancements in mechanical deflection performance, reduction in crosstalk, and improvement in scanning capability position it as a promising candidate for advanced optical systems. Future work should focus on experimentally verifying these simulation results and exploring potential applications in fields such as laser scanning and optical communication.

5 REFERENCES

[1] Liu, S., Zhang, G., Meng, L., Geng, S., & You, Z. (2024). Magnetic field density concentrated permanent magnet structure for electromagnetic MEMS scanning mirror. *Sensors and Actuators a Physical*, *373*, 115390-115390. https://doi.org/10.1016/j.sna.2024.115390

[2] Peng, A., Qiao, D., Xia, C., Song, X., & Liu, Y. (2024). Acc urately estimating the scanning angle of an electrostatic ME -MS mirror with a novel damping model. *Sensors and Actua -tors a Physical*, *37*, 115392-115392. https://doi.org/ 10.1016/j.sna.2024.115392

[3] Du, Y., Wu, D., Song, Z., Liu, M., Yang, S., & Wang, Z. (2016). 3-D Integration of MEMS and CMOS Using Electroless Plated Nickel Through-MEMS-Vias. *Journal of Microelectromechanical Systems*, *25*(4), 770-779. https://doi.org/10.1109/jmems.2016.2563522

[4] References Wang, Y., Uchida, K., Munenori Takumi, Ishii, K., & Kitayama, K. (2024). Reservoir computing for a ME-MS mirror-based laser beam control on FPGA. *Optical Revi ew*, *37*(4). 111-115.

[5] Zhang, G., Wang, X., Wang, Y., Cui, H., Zhao, W., & Qiu, L. (2024). Miniaturized high-resolution dual 2D MEMS mirror scanning confocal Raman microscopy for topographic and Raman mapping. *Measurement*, *224*, 113807-113807. https://doi.org/10.1016/j.measurement.2023.113807

[6] Matteo Manzotti, Rezvani, Z., Immacolata Pedaci, Paola Sabrina Barbato, Balsamo, A., Losa, S., & Casuscelli, V. (2023). Prediction of the drift trend in piezoelectrically actuated MEMS mirror by 2D reliability modelling. *Microelectronics Reliability*, *150*, 115228-115228. https://doi.org/10.1016/j.microrel.2023.115228

[7] Iizuka, A., Choe, S., Hashizume, J., Yasuhiro Itou, & Okada, R. (2011). Development of two - axis electromagnetic driving MEMS mirror. *Electronics and Communications in Japan*, *94*(11), 18-23. https://doi.org/10.1002/ecj.10378

[8] Zhu, J., Liu, X., Shi, Q., He, T., Sun, Z., Guo, X., Lee, C. (2019). Development Trends and Perspectives of Future Sensors and MEMS/NEMS. *Micromachines*, *11*(1), 7-10. https://doi.org/10.3390/mi11010007

[9] Jiang, B., Peng, M., Liu, Y., Zhou, T., & Su, Y. (2019). The fabrication of 2D micromirror with large electromagnetic driving forces. *Sensors and Actuators A: Physical*, *286*, 163-168. https://doi.org/10.1016/j.sna.2018.12.038

[10] Cheng-You, Y., Bo, L., & Zhen, Q. (2019). 2D Au-Coated Resonant MEMS Scanner for NIR Fluorescence Intraoperative Confocal Microscope. *Micromachines*, 5, 295-295.

[11] Yao, C. Y., Li, B., & Qiu, Z. (2019). 2D Au-Coated Resonant MEMS Scanner for NIR Fluorescence Intraoperative Confocal Microscope. *Micromachines*, *10*(5), 295-297. https://doi.org/10.3390/mi10050295

[12] Luo, S., Wang, D., Tang, J., Zhou, L., Duan, C., Wang, D., Xie, H. (2018). Circumferential-scanning endoscopic optical coherence tomography probe based on a circular array of six 2-axis MEMS mirrors. *Biomedical Optics Express*, *9*(5), 2104-2104. https://doi.org/10.1364/boe.9.002104

[13] Liu, L., Pal, S., & Xie, H. (2012). MEMS mirrors based on a curved concentric electrothermal actuator. Sensors and Ac -tuators A: *Physical*, *188*, 349-358. https://doi.org/10.1016/j.sna.2012.03.021

[14] Pallapa, M. & Yeow, J. T. W. (2013). Design, Fabrication and Testing of a Polymer Composite Based Hard-Magnetic Mirror for Biomedical Scanning Applications. *Journal of the Electrochemical Society*, *161*(2), B3006-B3013. https://doi.org/10.1149/2.001402jes

[15] Zhou, Y., Wen, Q., Wen, Z., & Yang, T. (2016). Modeling of MOEMS electromagnetic scanning grating mirror for NIR micro-spectrometer. *AIP Advances*, *6*(2), 16-18. https://doi.org/10.1063/1.4942973

[16] Cai, H., Zhang, X. M., Lu, C., Liu, A. Q., & Khoo, E. H. (2005). Linear MEMS variable optical attenuator using refle ct-ive elliptical mirror. *IEEE Photonics Technology Letters*, *17*(2), 402-404. https://doi.org/10.1109/lpt.2004.840056

[17] Park, Y., Moon, S., Lee, J., Kim, K., Lee, S.-J., & Jong Hyun Lee. (2018). Via-Less Two-Axis Electromagnetic Micro Scanner Based on Dual Radial Magnetic Fields. *IEEE Photonics Technology Letters*, *30*(5), 443-446. https://doi.org/10.1109/lpt.2018.2797269

[18] Samuelson, S. R. & Xie, H. (2014). A Large Piston Displacement MEMS Mirror With Electrothermal Ladder Actuator Arrays for Ultra-Low Tilt Applications. *Journal of Microelectromechanical Systems*, *23*(1), 39-49. https://doi.org/10.1109/jmems.2013.2290994

[19] Mohammad, T., He, S., & Mrad, R. B. (2021). Analysis of Optical Diffraction Profiles Created by Phase-Modulating MEMS Micromirror Arrays. *Micromachines*, *12*(8), 891. https://doi.org/10.3390/mi12080891

[20] Wang, X., Xie, Y., Liang, H., & Zhong, N. (2021). Analysis of Distortion Based on 2D MEMS Micromirror Scanning Projection System. *Micromachines*, *12*(7), 818. https://doi.org/10.3390/mi12070818

[21] Liu, S., Zhang, G., Meng, L., Geng, S., & You, Z. (2024). Magnetic field density concentrated permanent magnet structure for electromagnetic MEMS scanning mirror. *Sensors and Actuators a Physical*, *373*, 115390-115390. https://doi.org/10.1016/j.sna.2024.115390

[22] Li, Q., Yang, Y., Yan, S., Zhang, B., & Wang, C. (2021). Real-time variable field-of-view scanning of LiDAR by controlling the drive voltage of MEMS micromirror. *Optik*, *246*, 167760. https://doi.org/10.1016/j.ijleo.2021.167760

[23] Mahmood Chahari, Mohammad TaghiAhmadian, &Keikh-osrowFiroozbakhsh. (2023). Nonlinear dynamic analysis ofelectrostatically actuated dual-axis micromirrors. *Journal of the Brazilian Society of Mechanical Sciences and Engin.*, *45* (3), 13-15. https://doi.org/10.1007/s40430-022-03948-3

Contact information:

Lin ZHANG
School of Electronic Information Engineering,
Geely University of China, Chengdu, 641423

Qian WANG
School of Electronic Information Engineering,
Geely University of China, Chengdu, 641423

Yuanlin XIA
(Corresponding author)
Sichuan University,
Chenghua District, Chengdu, China
E-mail: yuanlin.xia@scu.edu.cn

YanTing XIA
School of Electronic Information Engineering,
Geely University of China, Chengdu, 641423

Lei ZHONG
Sichuan University,
Chenghua District, Chengdu, China